Available online at www.sciencedirect.com
SCIENCE DIRECT
Journal of Catalysis 238 (2006) 361–368
JOURNAL OF CATALYSIS
www.elsevier.com/locate/jcat

Adsorption and desorption analysis of NO_x and SO_x on a Pt/Ba thin film model catalyst

Y. Sakamoto *, K. Okumura, Y. Kizaki, S. Matsunaga, N. Takahashi, H. Shinjoh

Toyota Central Research & Development Labs, Inc. Nagakute, Aichi, 480-1192, Japan

Received 20 September 2005; revised 12 December 2005; accepted 22 December 2005

Available online 27 January 2006

Abstract

A NO_x storage and reduction catalyst for automotive exhaust gas was investigated using a model catalyst consisting of a Pt/Ba thin film on a Si substrate. The NO_x or SO_x adsorption/desorption phenomena in the model catalyst were studied using EPMA, AES, XPS, and EELS by changing the treatment conditions, temperature, and atmosphere. Based on measuring the nitrogen and sulfur distributions, the following results were found: NO_x was strongly adsorbed around an edge of platinum, and SO_x was adsorbed on a barium oxide layer independent of the platinum distribution. The NO_x adsorption around the platinum edge within a few micrometers was preferentially decreased; and the SO_x adsorption around the platinum edge was decreased for a distance of a few nanometers. These visual results for NO_x and SO_x adsorption/desorption provided supporting evidence for the phenomenon occurring during practical use of NO_x storage and reduction catalysts in the purification for automotive exhaust gases.

Keywords: Sulfur poisoning; Lean-burn engine; NO_x storage-reduction catalyst; Platinum; Barium

1. Introduction

Lean-burn engines and diesel engines are widely used to save fuel costs and to decrease vehicle emissions, such as CO_2. However, cleaning up NO_x exhaust emissions produced by engines under excess oxygen conditions is difficult. Scientists have been studying NO_x elimination systems for many years. Recently, a system using a NO_x storage and reduction (NSR) catalyst has been identified and developed as one of the best systems for eliminating NO_x under excess oxygen conditions [1,2]. NSR catalysts can eliminate NO_x under excess oxygen conditions by storing the NO_x in "NO_x storage materials," such as barium oxide, sodium oxide, and potassium oxide. The stored NO_x is then reduced to N_2 under appropriate conditions involving such reducing gases as H_2, CO, and hydrocarbons. Through repetition of this cycle of NO_x storage and reduction, the NSR catalyst purifies the NO_x.

NSR catalysts are considered a significant technology for NO_x purification and are now widely used. However, NO_x storage materials have been found to undergo a reaction whereby they also convert SO_x to sulfate and thereby lose the ability to store NO_x [3]. This so-called "SO_x poisoning" is recognized as one of the greatest problems hindering the wider use of NSR catalysts, and ways to overcome the SO_x poisoning effect have been widely studied [4,5]. SO_x poisoning can be removed using the following reactions, shown here with barium oxide as an example:

$$BaSO_4 + H_2 \rightarrow BaO + SO_2 + H_2O$$

and

$$BaSO_4 + 4H_2 \rightarrow BaO + H_2S + 3H_2O.$$

We believe that there are four important reactions besides SO_x poisoning and recovery to consider when applying the NSR as an automotive exhaust: NO_x adsorption, NO_x desorption, SO_x adsorption, and SO_x desorption. Various studies have investigated these four reactions, leading to the following observations:

- The spillover of NO_x between the precious metal and the NO_x storage material plays an important role [6–8].

* Corresponding author. Fax: +81 561 63 5260.
E-mail address: sakamoto@mosk.tytlabs.co.jp (Y. Sakamoto).

0021-9517/$ – see front matter
doi:10.1016/j.jcat.2005.12.025

- The desorbed NO_x is reduced to N_2 over a precious metal [1,9,10].
- The smaller the crystallite size of the sulfate, the greater the rate of SO_x desorption and recovery of the NO_x storage material [11–14].
- The inclusion of precious metals accelerates the SO_x desorption reaction [12–14].

We also need to understand the spillover of NO_x, SO_x, and the reducing gas, because the four reactions apparently occur mainly around the precious metal–NO_x storage material interface. But such studies have not yet been widely performed, with the exception of investigations into the size of the precious metal and the barium oxide particles. Rigorously preparing an adequate model catalyst for the analysis of the spillover and arrange the precious metal and the NO_x storage material will provide valuable information for developing an NSR catalyst. However, analyzing the geometry has proven difficult, because the commonly used powder catalysts are very complicated and unsuited to investigating the spillover phenomenon. Hence we believed that for this analysis it would be more appropriate to design a simpler model catalyst on a flat substrate using thin film technology.

Our goal in this study is to obtain an image of the NO_x and SO_x reactions with reference to the arrangement of the precious metal and the NO_x adsorption material. In particular, we wish to derive the relationship for the distance between the precious metal and the NO_x adsorption material for each reaction. These results will be of assistance in developing an NO_x storage catalyst. Therefore, we performed a study of a simple model catalyst using a flat substrate and a thin film using electron probe microanalysis (EPMA), scanning electron microscopy (SEM), transmission electron microscopy (TEM), electron energy loss spectrometry (EELS), X-ray photoelectron spectroscopy (XPS), and Auger electron spectrometry (AES).

2. Experimental

2.1. Preparation of model catalysts

Barium oxide was selected as the NO_x storage material, and platinum was selected as the precious metal. Barium oxide was deposited to a thickness of 200 nm on a Si(110) substrate by a sputtering method using a barium peroxide target. After the barium oxide deposition, a 10 nm thick platinum layer was deposited through a 50 μm square-hole mask composed of Ni with a rectangular shape 0.5 cm in size. The thickness of the barium oxide and the platinum were estimated using a combination of a crystal vibration method and the time taken for deposition. The Si substrate was rotated during the barium oxide deposition for a flat film but was not rotated during the Pt deposition for the shape edge of Pt. Because of the differences in the rotation of the Si substrate, the thickness of the Ba film becomes uniform; however the thickness of each Pt-deposited square island differed depending on location. Fig. 1 illustrates the Pt/BaO_x/Si model catalyst used for the EPMA, SEM, XPS, and AES analyses. We define this sample (before any subsequent treatment) as the "fresh state."

Fig. 2 shows an SEM image of the Pt/BaO_x/Si model catalyst in the fresh state before any treatment. The smooth bright area is the site of the Pt deposition, which has a rounded edge. The surface of the area of Ba deposition was not smooth, appearing more like fish scales. The distributions of the Pt and Ba were mapped as an EPMA image, as shown in Fig. 3. The distribution of the Pt on the left side was sharp, whereas the distribution on the right side was broader because the Pt was deposited from the left direction through a shadow mask. The shape of the Pt deposition on the left edge of the shadow mask was clear, but on the right side of the mask the evaporated Pt atoms could encroach into the space between the mask and the Si substrate. The BaO_x film was thinner around the edge of the Pt than in the other areas, due to the Pt deposition. The surface distribution of Pt and Ba was mapped by AES (Fig. 4), which is considered an appropriate surface analysis technique. The surface distribution of the Pt was sharper than the bulk distribution measured by EPMA, and Ba was detected in all areas except those in which Pt deposition occurred. Because it is recognized that the model catalyst obtained thusly is almost the same as

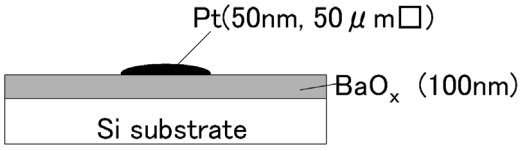

Fig. 1. Pt/BaO_x/Si model catalyst for EPMA and AES analysis.

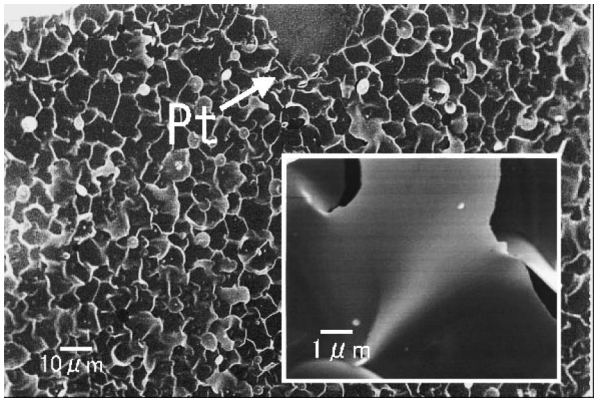

Fig. 2. SEM image of Pt/BaO_x/Si model catalyst.

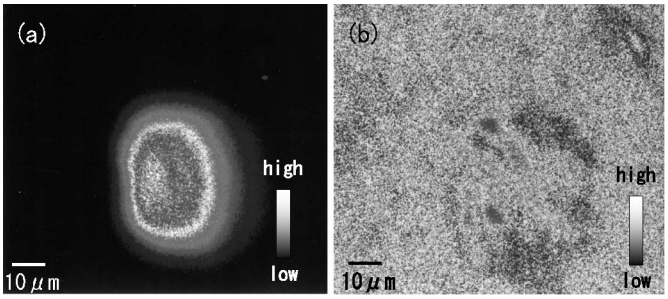

Fig. 3. EPMA image of Pt/BaO_x/Si model catalyst: (a) Pt and (b) Ba distribution.

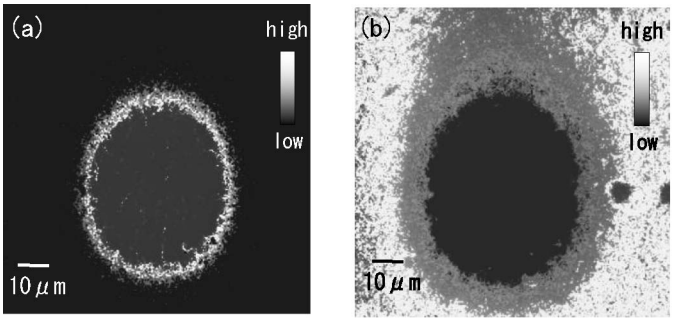

Fig. 4. AES image of Pt/BaO_x/Si model catalyst: (a) Pt and (b) Ba distribution.

that shown in Fig. 1 in the micrometer range, we decided to perform further analysis of the NSR catalyst reaction.

AES was originally considered an appropriate method for measuring the distribution of Pt, Ba, N, and S because its sensitivity and spatial resolution are superior to that of EPMA. But in this instance, we had to revise our ideas about using AES as a method for analyzing the distribution of these elements. The electron beam used as the probe in AES caused some blackening of the areas with low distributions of Ba, except for the areas in which Pt was deposited. It is concluded that in our experiment AES can be used for the Pt area analysis but not for the barium area, because the electron beam is believed to damage and contaminate the barium oxide. The results of the AES analysis seem to be affected by contamination and the state of the barium oxide; therefore, EPMA was the main analysis technique.

2.2. Gas treatment and characterization of model catalysts

The model catalyst was found to be adequate for our analysis; therefore, we treated the model catalyst with four sets of conditions to simulate the four reactions that are important in the production of a practical NSR catalyst: NO_x adsorption, NO_x desorption, SO_x adsorption, and SO_x desorption.

The NO_x treatment used to simulate the NO_x adsorption was as follows. The Pt/BaO_x/Si model catalyst was heated in an NO_x atmosphere at 476, 573, and 673 K for 1 h to store NO_x in the model catalyst. A reduction process under H_2 was then carried out to simulate NO_x desorption, as follows. The Pt/BaO_x/Si model catalyst that had been heated in NO_x was further heated at 523 and 623 K in an H_2 atmosphere for 1 h to release the stored NO_x from the model catalyst. The details of each of these atmospheres are summarized in Table 1. The surface shapes of these model catalysts were observed using SEM. The bulk distributions of Pt and Ba around each sample were measured using EPMA.

The simulated SO_x treatment was as follows. The Pt/BaO_x/Si model catalyst was heated in a SO_x atmosphere at 573, 673, 773, and 873 K for 1 h to adsorb SO_x onto the model catalyst. After the SO_x treatment, the Pt/BaO_x/Si model catalyst was heated in an H_2 atmosphere at 873, 923, and 973 K for 30 min to simulate the SO_x desorption.

After the above treatments, each sample was analyzed using a two-dimensional analysis by EPMA and AES. Each sample was also analyzed to reveal the extent of the NO_x and SO_x diffusions into the BaO_x thin film. This depth information was obtained to compare the molar ratios of N/Ba and S/Ba obtained by EPMA and XPS, because EPMA measures to a micrometer depth, whereas XPS measures to a depth of a few nanometers. The molar ratio of N/Ba indicates the ratio of "NO_x storage barium oxides" to "free barium oxides" (those not used to store NO_x). The same approach was adapted to determine SO_x adsorption and release by measuring the molar ratio of S/Ba.

Table 1
Treatment atmosphere

Treatment	Atmoshpere
NO_x	NO 2%:N_2 350 cc/min, NO (2%) 100 cc, O_2 50 cc
SO_x	SO_x 0.2%:N_2 800 cc/min, SO_2 (2%) 100 cc, O_2 100 cc
H_2	H_2 5%:N_2 950 cc/min, H_2 50 cc

Oxidizing conditions for a few minutes and reducing conditions for a few seconds were alternately repeated to eliminate NO_x in exhaust gas simulating realistic engine operation. The treatment duration of our experiment, one hour, seems to be longer than that of realistic engine operation. We suppose that the long duration of our experiment is suitable for a duration test; an automotive catalyst is usually used for about 10,000 h. Analysis of the shorter duration is interesting and is affected more by the surface of barium nitrate [15] and sulfate [16]. The shorter duration time decreases the amounts of nitrate and sulfide, making it more difficult to measure the distribution of N and S. Other methods for surface analysis may be needed.

Regarding gas conditions, practical exhaust gases involve CO_2 and H_2O. The kinds of gas have some affect on NSR [17–19] and merit investigation. We consider the study of treatment duration and gas conditions subjects of future investigation using this model catalyst.

3. Results

3.1. NO_x adsorption and reduction of the Pt/BaO_x/Si model catalyst

An appropriate model catalyst was obtained, and the NO_x adsorption and reduction over the Pt/BaO_x/Si model catalyst were investigated. Fig. 5 shows an SEM image of the model

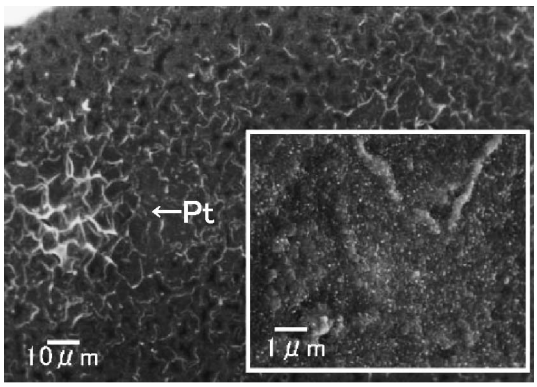

Fig. 5. SEM image of Pt/BaO_x/Si model catalysis after 673 K NO_x treatment.

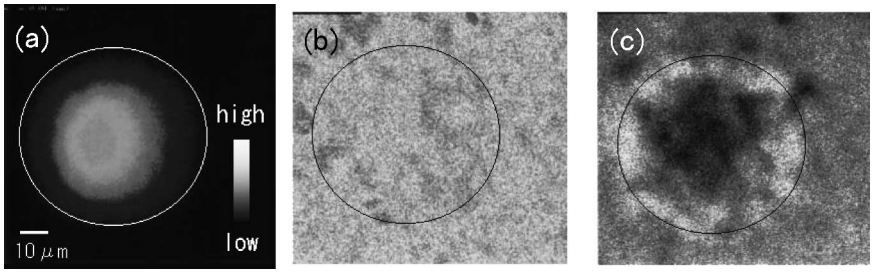

Fig. 6. EPMA image of Pt/BaO_x/Si model catalyst after 673 K NO_x treatment: (a) Pt, (b) Ba and (c) N distribution.

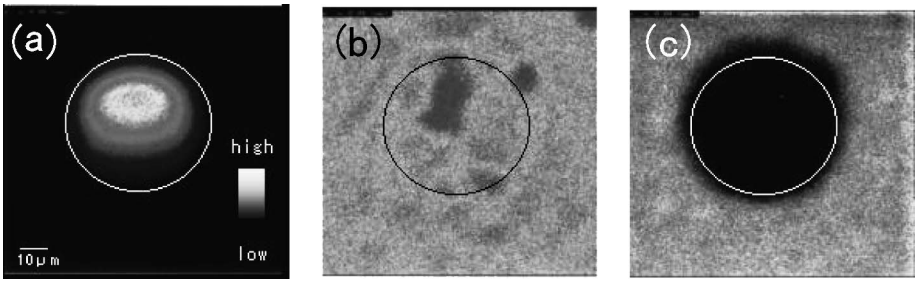

Fig. 7. EPMA image of Pt/BaO_x/Si model catalyst after 673 K NO_x treatment followed by 523 K H_2 treatment: (a) Pt, (b) Ba and (c) N distribution.

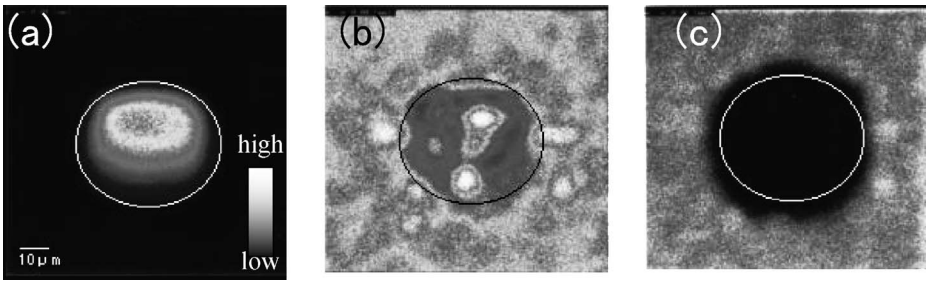

Fig. 8. EPMA image of Pt/BaO_x/Si model catalysis after NO_x treatment followed by 623 K H_2 treatment: (a) Pt, (b) Ba and (c) N distribution.

catalyst after the NO_x treatment. The surface of the Ba became smoother and the contrast with the Pt area became weaker than in the fresh state before treatment in the image with the 10-μm scale bar in Fig. 5. Small particle sizes of Ba became visible at higher magnification as shown in the image with the 1-μm scale bar in Fig. 5. Similar picture of small particles on flat large planes after the NO_x treatment is also reported as small $Ba(NO_3)_2$ particles on stable flat $Ba(NO_3)_2$ particles in NSR catalyst using BaO/Al_2O_3 catalyst [20].

The distributions of Pt, Ba, and N were mapped as an EPMA image, as shown in Fig. 6. The white circle indicates an area in which Pt was detected. N was detected over the entire sample, and the concentration of N seemed to be higher around the edge of the Pt than in the other regions. The edge of the Pt area became blurred in comparison with its appearance before the NO_x treatment.

Samples of the Pt/BaO_x/Si model catalyst that had been treated by the NO_x treatment described above were reduced under H_2 at either 523 or 623 K. The results of these processes are shown in Figs. 7 and 8. The NO_x stored in the model catalyst was reduced in and around the Pt area. The width of the reduced material around the Pt was a few micrometers in both cases. When the H_2 treatment temperature was increased to 623 K (Fig. 8), the distribution of Ba became nonuniform.

3.2. SO_x adsorption and reduction above the Pt/BaO_x/Si model catalyst

The SO_x adsorption and reduction were also investigated for the Pt/BaO_x/Si model catalyst using the same technique used for the NO_x adsorption and reduction analysis. Fig. 9 shows an SEM image of the Pt/BaO_x/Si model catalyst after the SO_x treatment at 673 K. The area around the Pt was blackened, and submicrometer-size particles appeared on the surface of the barium area, as shown in the image with the 1-μm scale bar in Fig. 5. The distribution of the S was mapped as the EPMA image shown in Fig. 10. S was detected all over the sample. We attempted to measure the distribution of S on the Pt using AES, because S may strongly adsorb on the surface of Pt [21,22]. But because no S was detected on the Pt surface, as shown in Fig. 11, we concluded that the S was adsorbed mainly on the barium oxide. Pt played an important role in oxidizing the NO to NO_2 in the NO_x adsorption, but did not take part in the SO_x adsorption. This finding

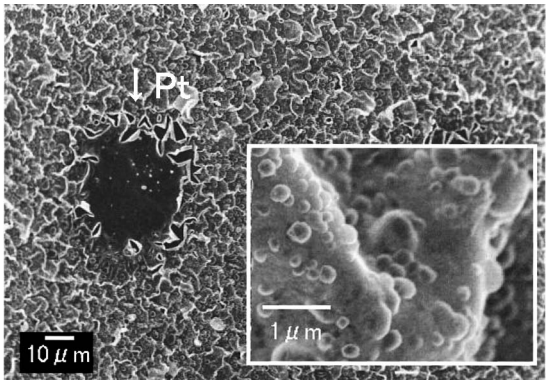

Fig. 9. SEM image of Pt/BaO_x/Si model catalyst after 673 K SO_x treatment.

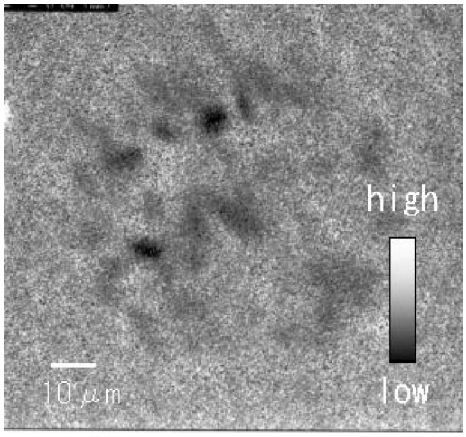

Fig. 10. S distribution measured by EPMA of Pt/BaO_x/Si model catalysis after 673 K SO_x treatment.

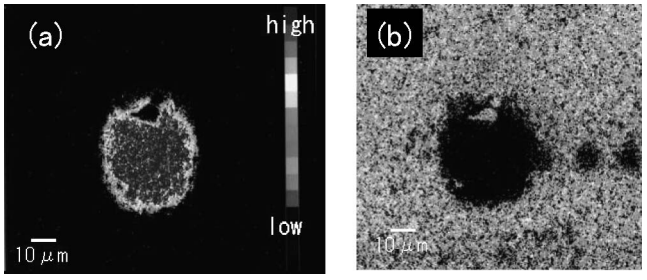

Fig. 11. AES image of Pt/BaO_x/Si model catalyst after 673 K SO_x treatment: (a) Pt and (b) S distribution.

was also reported in a number of studies on the sulfur deactivation of alumina-supported Pt catalysts that found that under lean conditions, SO_2 is oxidized to SO_3 independent of Pt [23].

The Pt/BaO_x/Si model catalyst that had undergone the SO_x treatment was reduced under H_2 at 873, 923, and 973 K. All of the EPMA results concerning the distributions of Pt, Ba, and S are shown in Fig. 12. The SO_x in the model catalyst was further reduced at increasing temperatures. The width of the area of the reduced S around the Pt was below the spatial resolution of the EPMA technique, which measures on a micrometer scale. A detailed analysis of the width of the SO_x desorption around the Pt was investigated using a nanoscale TEM analysis of the BaO_x/Pt/Al_2O_3 model catalyst.

3.3. SO_x reduction over a BaO_x/Pt/Al_2O_3 model catalyst on an Au mesh

The width of the SO_x reduction area of $Ba(SO_4)_2$ around the Pt could not be clarified by the EPMA analysis, because it was considered below the micrometer scale based on the resolution of the EPMA instrument. Therefore, the width of the SO_x reduction area around the Pt was investigated by TEM analysis with nanometer resolution.

Fig. 13 shows the BaO_x/Pt/Al_2O_3 model catalyst used for the TEM analysis. The model catalyst was produced as follows. An 80 nm film of Al_2O_3 was deposited by a sputtering method onto a NaCl crystal. The Al_2O_3 film was peeled off in water, from which the floating Al_2O_3 film was skimmed off using an Au mesh. This mesh was then treated in air at 873 K for 1 h, after which a 0.2 nm Pt layer was also deposited on the mesh by a sputtering method and treated in air at 873 K for 1 h to create Pt particles. A 1.8 nm layer of barium oxide was then deposited on this Pt/Al_2O_3 and treated in air at 873 K for 1 h. The Ba/Pt/Al_2O_3 model catalyst was analyzed by TEM with EELS capability (HF-2200, Hitachi High Technologies) after SO_x treatment and subsequent H_2 treatment. The SO_x treatment was performed at 673 K in SO_x atmosphere (as indicated in Table 1) for 30 min, and the subsequent H_2 treatment was performed at 873 K in H_2 atmosphere for 30 min.

Fig. 14 shows a TEM image and EELS images of the BaO_x/Pt/Al_2O_3 model catalyst after SO_x treatment at 673 K. Ba was uniformly deposited, and SO_x was adsorbed on the BaO_x. Fig. 15 shows a TEM image and EELS images of the BaO_x/Pt/Al_2O_3 model catalyst after SO_x treatment at 673 K followed by an H_2 treatment at 873 K. Because the area where the Pt existed was almost the same as the area of decreased S (by TEM analysis with nanometer resolution), the SO_x desorption was confirmed as occurring easily in a confined area of less than a few nanometers around the Pt.

3.4. Diffusion of NO_x and SO_x into the BaO_x thin film

Fig. 16 shows a comparison between the bulk and the surface distributions of N and S (measured by EPMA and XPS) in the Pt/BaO_x/Si model catalyst after the NO_x and SO_x treatments. The intensities of the N and S signals were normalized to commercially available $Ba(NO_3)_2$ and $BaSO_4$ (Kojundo Chemical Laboratory). Surface N/Ba and S/Ba ratio were always considered higher than the bulk ratios, because both NO_x and SO_x gas were contacted with the Ba oxide surface. The surface distribution of N was almost proportional to the bulk distribution, as shown in Fig. 16a; however, the surface distribution of S was not proportional at low temperature (below 773 K). The bulk distribution of S became proportional to the surface distribution at high temperature (873 K). This fact indicated that NO_x was uniformly adsorbed into the BaO_x, whereas SO_x was adsorbed from the surface of the BaO_x at low temperature.

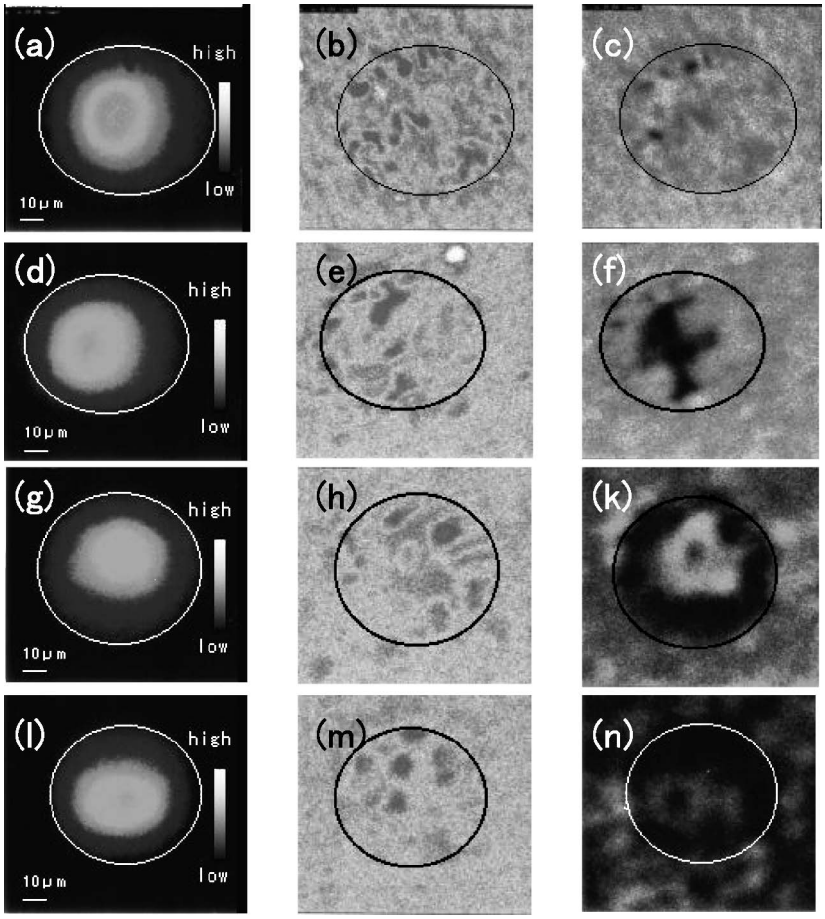

Fig. 12. EPMA image of Pt/BaO_x/Si model catalyst; after 673 K SO_x treatment, (a) Pt, (b) Ba and (c) S distribution; after the SO_x treatment followed by 873 K H_2 treatment, (d) Pt, (e) Ba and (f) S distribution; after 923 K H_2 treatment, (g) Pt, (h) Ba and (k) S distribution; after 973 K H_2 treatment, (l) Pt, (m) Ba and (n) S distribution.

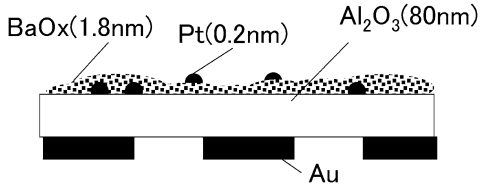

Fig. 13. BaO_x/Pt/Al_2O_3 model catalyst for TEM analysis.

4. Discussion

The differences among four main reactions—NO_x adsorption, NO_x desorption, SO_x adsorption, and SO_x desorption—must be considered when designing a practical NSR catalyst for automotive exhaust. NO_x adsorption, termed "NO_x storage" in this context, occurs as follows. NO is oxidized to NO_2, and the NO_2 reacts with barium oxides or barium carbonate to form barium nitrate. This mechanism is adapted for the SO_x adsorption. SO_x adsorption, termed "SO_x poisoning" in this context, reduces NO_x storage capability.

The strongest adsorption sites for NO_x and SO_x are considered to be those around the Pt. NO_x seemed to be adsorbed more readily around Pt than at the other sites (Fig. 7c); however, SO_x was adsorbed on the BaO_x regardless of the presence or absence of Pt.

The decomposition of $Ba(NO_3)_2$ was suggested to occur first within a few micrometers around the Pt (Fig. 8). This image,

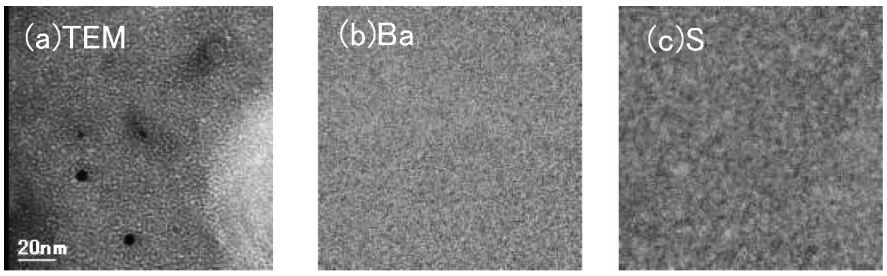

Fig. 14. TEM image and EELS image of BaO_x/Pt/Al_2O_3 model catalyst; after 673 K SO_x treatment, (a) TEM, (b) Ba and (c) S distribution; the dark area indicates low concentration.

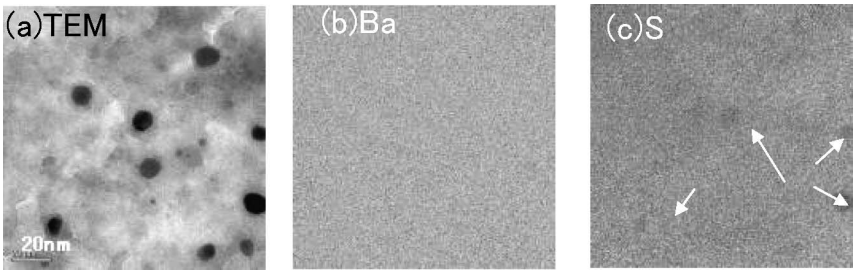

Fig. 15. TEM image and EELS image of $BaO_x/Pt/Al_2O_3$ model catalyst; after 873 K H_2 treatment followed by 673 K SO_x treatment: (a) TEM, (b) Ba and (c) S distribution, the dark area indicates low concentration.

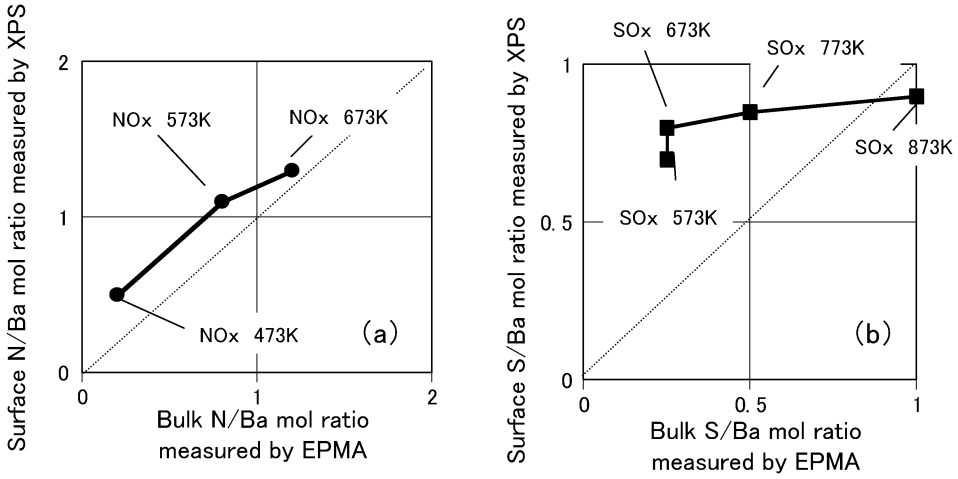

Fig. 16. Comparison between bulk and surface distribution of N and S measured by EPMA and XPS of $Pt/BaO_x/Si$ model catalyst.

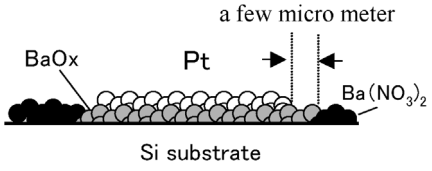

Fig. 17. View of reduction of $Ba(NO_3)_2$ around Pt.

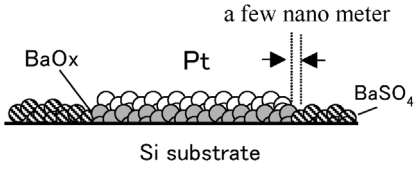

Fig. 18. View of reduction of $BaSO_4$ around Pt.

shown in Fig. 17, may provide insight into why only 20% of the Ba compound seems to work as an NO_x storage material immediately after the catalysts are produced [24]. The amount of NO_x storage depends on the number and size of the precious metal particles. When the amount of precious metal increases, the $Ba(NO_3)_2$ decomposition area increases, and when the particle size increases, the NO_x reduction area decreases. It has also been recently suggested that a "special area" of NO_x decomposition exists around the Pt particles [6,14,25].

It has been suggested that the reduction of $BaSO_4$ occurs within a few nanometers around the Pt as opposed to within a few micrometers of the $Ba(NO_3)_2$ decomposition. Two types of barium sulfates have been identified, bulk and surface, and platinum does not influence the reduction of bulk barium sulfates [17,26]. The difficulty eliminating S from $BaSO_4$ is reportedly caused by the formation of BaS on reducing condition, which is stable even at high temperature (1073 K) [11]. The reduction scheme for the $BaSO_4$ could be as illustrated in Fig. 18. The amount of Ba compounds that act as NO_x storage materials decreases under normal engine operation, including the SO_x regeneration process. Barium compounds within a few nanometers around the Pt can ultimately work as NO_x storage materials.

The differences in the decomposition processes of $Ba(NO_3)_2$ and $BaSO_4$ can be attributed to a spillover of hydrogen atoms. The currently accepted hydrogen spillover mechanism involves the migration of hydrogen atoms from a metal, which enables the dissociation of hydrogen molecules toward the acceptor material [27,28]. In particular, the decomposition of small $BaSO_4$ crystallites can be affected by hydrogen spillover [26]. The active hydrogen atoms are created on the Pt site and the spillover hydrogen atoms move toward the surface of the $Ba(NO_3)_2$ or $BaSO_4$. This model is essentially the same as that for H_2 on Pt/TiO_2 [29,30]. The difference in area between these two kinds of reduction may be caused by the mobility of the hydrogen atoms and the reactivity of the hydrogen atoms with the $Ba(NO_3)_2$ or the $BaSO_4$. Alternatively, the differences may be due to the differences in NO_2 and SO_3 spillover, because it has been reported that NO migration may originate from the

decomposition of barium nitrate to the noble metal sites via spillover [7]. For an NO_x storage catalyst to maintain a high activity as an NSR catalyst, the interface area between the Pt and the barium compounds must remain high.

Finally, we discuss in more detail the bulk and surface distributions of N/Ba and S/Ba ratio in the $Pt/BaO_x/Si$ model catalyst after NO_x and SO_x treatments, as shown in Fig. 16. It is well known that in the presence of SO_2, bulk sulfate is readily formed in these systems [14–16,21,27]. However, under normal operating conditions of oscillating lean/rich cycles, there is little evidence that bulk nitrates are formed [20,31]. At first glance, these findings seem to contradict those shown in Fig. 16; however, these differences can be reconciled by distinguishing between the surface of particles and the surface (top) of film. The film of barium oxide in the model catalyst is composed of small barium oxide particles, and the findings in the literature are adapted to these small particles. The small particles can readily become bulk sulfate in sequence from the surface of the film in the SO_x. It is difficult for SO_x to reach the bottom of film. On the other hand, only the surface of each particle can form nitrate. The BaO_x film gradually becomes barium nitrate from the top to the bottom at low temperature.

5. Conclusion

Thin film was designed as a NO_x storage catalyst and investigated with respect to NO_x and SO_x adsorption/desorption using EPMA, AES, XPS, and EELS. NO_x and SO_x were adsorbed all over the model catalyst; however, NO_x desorption occurred preferentially in an area a few micrometers around the platinum and was suppressed at all other sites, whereas SO_x desorption occurred preferentially in an area a few nanometers wide around the platinum.

Acknowledgments

The authors thank Mrs. Amano and Mr. Suzuki (Toyota Central Research & Development Labs) for the EPMA and TEM analysis.

References

[1] N. Takahashi, H. Shinjoh, T. Iijima, T. Suzuki, K. Yamazaki, K. Yokota, H. Suzuki, N. Miyoshi, S. Matsumoto, T. Tanizawa, T. Tanaka, S. Tateishi, K. Kasahara, Catal. Today 27 (1996) 63.
[2] W.S. Epling, L.E. Campbell, A. Yezerets, N.W. Currier, J.E. Parks, Catal. Rev. Sci.-Eng. 46 (2) (2004) 163.
[3] P. Engström, A. Amberntsson, A. Skoglundh, E. Fridell, G. Smedler, Appl. Catal. B 22 (1999) L241.
[4] S. Matsumoto, Catal. Today 90 (2004) 183.
[5] K. Yamazaki, T. Suzuki, N. Takahashi, K. Yokota, M. Sugiura, Appl. Catal. B 30 (2001) 459.
[6] L. Olsson, E. Fridell, M. Skoglundh, B. Andersson, Catal. Today 73 (2002) 263.
[7] S. Salasc, M. Skoglundh, E. Fridell, Appl. Catal. B 36 (2002) 145.
[8] P.T. Fanson, M.R. Horton, W.N. Delgass, J. Lauterbach, Appl. Catal. B 46 (2003) 393.
[9] R. Burch, J.A. Sullivan, J. Catal. 182 (1999) 489.
[10] R. Burch, A.A. Shestov, J.A. Sullivan, J. Catal. 182 (1999) 497.
[11] S. Poulston, R.R. Rajaram, Catal. Today 81 (2003) 603.
[12] A. Amberntsson, M. Skoglundh, M. Jonsson, E. Fridell, Catal. Today 73 (2002) 279.
[13] S. Matsumoto, Y. Ikeda, H. Suzuki, M. Ogai, N. Miyoshi, Appl. Catal. B 25 (2000) 115.
[14] Z. Liu, J.A. Anderson, J. Catal. 224 (2004) 18.
[15] Y. Su, M.D. Amiridis, Catal. Today 96 (2004) 31.
[16] Z. Liu, J.A. Anderson, J. Catal. 228 (2004) 243.
[17] S. Elbouazzaoui, E.C. Corbos, X. Courtois, P. Marecot, D. Duprez, Appl. Catal. B 61 (2005) 236.
[18] W.S. Epling, J.E. Parks, G.C. Campbell, A. Yezerets, N.W. Currier, L.E. Campbell, Catal. Today 96 (2004) 21.
[19] S. Balcon, C. Potvin, L. Salin, J.F. Tempère, G. Djéga-Mariadassou, Catal. Lett. 60 (1999) 39.
[20] J. Szanyi, J.H. Kwak, J. Hanson, C. Wang, T. Szailer, C.H.F. Peden, J. Phys. Chem. B 109 (2005) 7339.
[21] Ch. Sedlmair, K. Seshan, A. Jentys, J.A. Lercher, Catal. Today 75 (2002) 413.
[22] A. Amberntsson, M. Skoglundh, S. Ljungström, E. Fridell, J. Catal. 217 (2003) 253.
[23] V. Meeyoo, D.L. Trimm, N.W. Cant, Appl. Catal. B 19 (1998) L101.
[24] I. Nova, L. Castoldi, L. Lietti, E. Tronconi, P. Forzatti, Catal. Today 75 (2002) 431.
[25] D. James, E. Fourre, M. Ishii, M. Bowker, Appl. Catal. B 45 (2003) 147.
[26] X. Wei, X. Liu, M. Deeba, Appl. Catal. B 58 (2005) 41.
[27] M. Boudart, Adv. Catal. 20 (1969) 153.
[28] W.C. Conner Jr., G.M. Pajonk, S.J. Teichner, Adv. Catal. 34 (1986) 1.
[29] D.D. Beck, J.M. White, J. Phys. Chem. 88 (1984) 174.
[30] D.D. Beck, J.M. White, J. Phys. Chem. 88 (1984) 2764.
[31] P. Broqvist, H. Grönbeck, E. Fridell, I. Panas, Catal. Today 96 (2004) 71.